Lab on a Chip

Accepted Manuscript

ROYAL SOCIETY OF CHEMISTRY

www.rsc.org/loc

Journal Name

ARTICLE TYPE

Cite this: DOI: 10.1039/xxxxxxxxxx

A continuous roll-pulling approach for the fabrication of magnetic artificial cilia with microfluidic pumping capability†

Ye Wang,[a,b,c] Jaap den Toonder,*[a,c] Ruth Cardinaels,[a] and Patrick Anderson[a,c]

Received Date
Accepted Date

DOI: 10.1039/xxxxxxxxxx

www.rsc.org/journalname

Magnetic artificial cilia are micro-hairs covering a surface that can be actuated using a time-dependent magnetic field to pump or mix fluids in microfluidic devices. This paper presents a novel fabrication method to realize magnetic artificial cilia using a roll-pulling process, in which a cylinder decorated with micro-pillars rolls over a liquid precursor film that contains magnetic particles at a speed up to 1 m/s, while a magnetic field is applied. Due to the interaction between the pillars and the liquid film, micro-hairs are pulled out of the film. In this way, surfaces with slender cone-shaped magnetic artificial cilia were produced. When integrated in a closed-loop channel, the artificial cilia were shown to be capable of generating substantial microfluidic pumping using external magnetic actuation. The spatial arrangement of the cilia can be varied by altering the layout of the micro-pillars on the roll surface. In addition, the final geometry of the individual cilia depends on the rheological properties of the precursor material in combination with the processing parameters of the roll-pulling process. A rheological study and fabrication tests were carried out for a range of precursor material compositions to obtain insight into the relation between precursor rheology and processing conditions on the one hand, and cilia geometry on the other hand. The development of this cleanroom-free, high speed and potentially large area method of production of artificial cilia is another step towards their implementation in real-life applications.

1 Introduction

In nature, microscopic hair-like structures are ubiquitous and perform varies functions such as fluid actuation, mechanical and chemical sensing, temperature regulation, and surface energy modification. A prominent example of such structures are eukaryotic cilia, which have hair-like geometries with a typical width of 200 nanometer and a length of 2 to 15 micrometer that can be found on the surface of certain cells.[1] *Paramecium*, a waterborne single cell organism, uses cilia covering its body to swim in water at a speed up to 1 mm/s, or ten times its body length per second. The epithelial cilia present in the inner linings of human lungs and trachea can sweep out mucus to prevent infection. Another example are flagella, which are longer but fewer than cilia, and can also provide motion for cells, e.g. sperm cells. Other types of 'micro-hairs' can have different functions. For example flies have hairy pads that allow them to cling on vertical or even inverted surfaces,[2] while water-striders have micro-hair covered legs that allow them to travel swiftly over water surfaces.[3]

Inspired by nature, micro-structures resembling cilia, typically referred to as 'artificial cilia' (ArtC), have been developed in recent years, most notably for microfluidic applications.[4] Evans *et al.* used track-etched membranes as sacrificial templates to fabricate Poly(dimethyl siloxane) (PDMS) based magnetic nanorods with a size close to that of natural cilia.[5] Vilfan *et al.* exploited the self-assembling ability of magnetic beads and created ArtC consisting of magnetically linked chains which were anchored to electroplated nickel dots.[6] The same mechanism was used by Babataheri *et al.* with the addition of a polymer coating (polyacrylic acid) to link the chains permanently to the substrate.[7] The ArtC reported above have cylindrical shapes, and they were actuated by external magnetic fields to perform a 3-D tilted conical motion, in an effort to mimic the movement of natural cilia. The maximum induced fluid flow speeds are in the order of micrometers per second. Using cleanroom microfabrication technologies, den Toonder *et al.*[8] fabricated electrostatically actuated beams, or 'flaps', about ten times bigger than natural cilia, and consisting of bilayer films of polyimide and chromium. These ArtC were integrated directly into a microfluidic channel and actuated elec-

[a] *Eindhoven University of Technology, P.O. Box 513, 5600 MB Eindhoven, the Netherlands. E-mail: J.M.J.d.Toonder@tue.nl*
[b] *Dutch Polymer Institute DPI, P.O. box 902, 5600 AX Eindhoven, the Netherlands*
[c] *Institute for Complex Molecular Systems, ICMS, De Zaale, 5612 AJ Eindhoven, the Netherlands*

† Electronic Supplementary Information (ESI) available: [details of any supplementary information available should be included here]. See DOI: 10.1039/b000000x/

trostatically between a bent and a flat state at frequencies up to 200 Hz, generating a substantial net flow velocity of more than 500 μm/s. Magnetic flap-like artificial cilia of similar dimensions were made by Belardi *et al.*[9] using an acrylic elastomer doped with superparamagnetic particles, and they could generate a net flow up to hundreds of μm/s when actuated using a rotating magnet.[10] Dreyfus *et al.*[11] made artificial flagella by attaching DNA connected magnetic beads to a red blood cell. In an oscillating magnetic field the flagella could perform a wave-like motion and drag the cell through liquid at a speed up to 5 μm/s. In other studies, light[12] and pH[13] responsive artificial flagella and cilia were also made, providing alternative means of actuation.

Besides being used to create fluid flow in microfluidics, ArtC can also be used for other applications such as mechanical/chemical sensing[14] and control of surface wettability.[15] Elastic micropillars such as artificial cilia made with PDMS with a well-defined geometry and known modulus can be used to measure mechanical forces induced by flow or by contact with solid substances. In fact some of the earliest artificial cilia were constructed for stress sensing in cell mechanics studies.[14,16] Similarly coherently patterned flexible micropillars made of PDMS were used for measuring wall shear stress and for characterization of turbulent flow patterns.[17] Chemical changes in the surrounding environment can also be detected by specially designed artificial cilia. Using a hydrogel that changes its volume upon pH changes as the base material for ArtC, pH values can be detected by monitoring the amplitude of magnetically actuated movement.[18] Micropillar arrays on a surface can also exhibit superhydrophobicity by minimizing the contact area between the surface and droplets on it. Due to the large contact angle of water droplets and the corresponding ease of droplet roll-off on such surfaces, self-cleaning surfaces inspired by the lotus leaf can be created.[19]

In most of the previously published work on ArtC, a big drawback for real applications is that the fabrication techniques adopted are tedious and costly, as they either require microfabrication techniques such as photolithography,[6,8,9,20,21] or rely on expensive sacrificial materials.[5] In order to address this issue, our research is aimed at fabricating artificial cilia in a cost-efficient, cleanroom-free manner, while realising an effective pumping function that can be practically used in lab-on-a-chip devices. Previously we reported two different cleanroom free techniques for the fabrication of artificial cilia. One described the fabrication of latex coated self-assembled ArtC, which were able to generate a net flow velocity of a few micrometers per second when actuated in a modest magnetic field (below 14 mT).[22] Later another fast and robust fabrication technique was presented, in which ArtC were created by magnetically drawing high aspect-ratio filaments out of a precursor layer. These ArtC were able to generate a net flow velocity of around a hundred micrometers per second with magnetic actuation using the same field strength.[23] Both techniques are more cost-effective and less tedious than the previously published fabrication approaches for artificial cilia, but they are still unsuitable for implementation in controlled large-scale fabrication. Especially scaling up to large area and continuous production is difficult, since the two methods rely on the generation of large magnetic field gradients which is in practice difficult to achieve over a large surface area.

In this paper, we present a completely new cleanroom-free high-speed fabrication technique, in which magnetic artificial cilia are produced in a continuous manner by point-wise drawing from a liquid precursor layer using a surface-modified roll, thereby significantly reducing fabrication cost and time, and allowing for scale up to continuous large area production. In this method, which shows some similarities with the roll-to-roll gravure printing process,[24] the cilia geometry depends on the breakup and retraction of the formed liquid bridge of precursor material. The latter processes can be tailored by means of the rheology of the precursor material and the processing conditions. The resulting ArtC can be magnetically actuated using a rotating magnet and can generate a significant flow in a microfluidic chip.

2 Fabrication of artificial cilia

2.1 Fabrication process and precursor material composition

An in-house developed setup was used to fabricate artificial cilia, as shown in Fig.1(a,b). The setup features a synchronized movement (through a rigid string) and an adjustable gap between a 10 cm long aluminium roll and a substrate holder, so that the line speed of the surface of the roll and the substrate are the same without any friction induced between them. The substrate can move at a speed between 2 mm/s and 1 m/s. A PDMS sheet with cylindrical micropillars made with soft-lithography (Fig.1c) is attached to the surface of the roll after plasma treatment; the micropillars are typically 200 μm wide and 300 μm long, and the base of the sheet is about 150 μm thick. A 200 μm thick liquid magnetic precursor layer was applied on a 75 mm by 75 mm glass substrate, which was then placed onto the substrate holder in the setup and fixed by vacuum. The composition of the precursor material is described below. As the substrate travels underneath the rotating roll, the micropillars touch the precursor film and pull out thin filaments from the film; these filaments reach a certain critical length before breaking. The extension rate of the filaments, determined by the diameter of the roll and the relative speed between the roll and the substrate, is typically in the order of hundreds per second. More details on the extension rate can be found in Supplementary Information. Subsequently, the remaining parts of the filaments on the substrate are thermally cured in an oven to produce ArtC. A pair of vertically aligned electromagnetic poles (surface area 10 cm x 10 cm) is fixed in the setup above and below the moving parts, in such a way that a uniform magnetic field up to 300 mT can be imposed in the area where the ArtC are formed. Fig.1d shows the final result of the roll pulling process, demonstrating that it is indeed possible to achieve large-area production of ArtC. The full scale image is shown in ESI.

The precursor material for the artificial cilia consists of a base fluid of thermally curable PDMS and a curing agent (Sylgard 184, Dow), a high molecular weight PDMS gum (molecular weight (MW) > 500,000, Gelest), iron particles (carbonyl iron powder, 99.5%, BASF), a PDMS-poly(ethylene oxide) block copolymer (PEO-b-PDMS, MW≈3000, Polysciences) and fumed silica

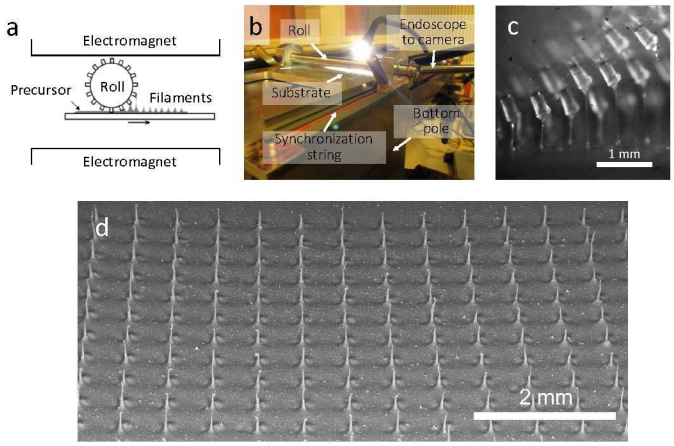

Fig. 1 (a) Schematic of the fabrication process; (b) picture of the fabrication setup showing the moving parts and an endoscope which is mounted on a high speed camera to capture the drawing of the filaments during the fabrication process; the synchronization string is used to drive the roll, so that the surface speed of the roll is synchronized with that of the substrate; the bottom electromagnetic pole can also be seen (top pole is removed in order to show the roll); (c) snapshot from high-speed imaging showing the PDMS micropillars on the surface of the roll serving as contact points; individual filament being pulled out from the substrate can be seen. A movie of the pulling process can be found in the Electronic Supplementary Information (ESI). (d) An array of artificial cilia taken from a 60 degree tilting angle using SEM (see full scale image in ESI).

nanoparticles (0.007 μm, no surface treatment, Cabot). The rheology of the precursor material was studied combined with fabrication experiments, which will be discussed in section 2.3, in order to produce sufficiently long ArtC. The hygroscopic silica particles were heated at 110 °C under vacuum for 1 hour to remove water before compounding. The mixture was mixed by hand for 10 min, and then degassed using a Thinky mixer (AR250, Artisan) at 2000 rpm for 2 min. The nominal size of the silica nanoparticles is 7 nanometers and they form aggregates of about 1 μm,[25] which is similar to the size of the iron particles and therefore can be considered sufficiently small for this application. The mixture was applied onto the 75 mm $\times$ 75 mm glass substrate using a film applicator (Erichsen GmbH & Co.), forming a precursor layer of typically 200 μm thick. The thickness of the precursor layer affects the length of the artificial cilia, therefore it was kept constant in the experiments in order to reduce the number of variables that affect the results. After filament drawing, the substrate was placed in an oven at 80 °C for 2 hours to thermally cure the PDMS and thus permanently fix the cilia shape.

2.2 The effect of an external magnetic field on the geometry of ArtC

As mentioned earlier, a pair of fixed electromagnets is placed symmetrically above and underneath the moving substrate. This allows to generate a magnetic field up to 300 mT perpendicular to the substrate at the location where the filaments are pulled out (see Fig.1a). The magnetic field applies an alignment force for the cilia to remain straight and perpendicular to the substrate. Fig.2 shows that with the field turned off, the tips of the artificial

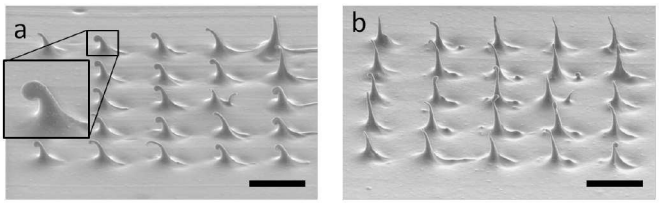

Fig. 2 The effect of the external magnetic field during roll pulling fabrication of artificial cilia. (a) Significant curling and collapsing happened when the electromagnets were turned off, which reduced the overall length; (b) artificial cilia remained straight and became longer when a vertical magnetic field (about 200 mT) was applied in the fabrication area (see the schematic in Fig. 1a). Both scale bars are 500 μm.

cilia tilted more and even curled back, which can cause a decrease in the length of the cilia and reduce their effectiveness during actuation. Therefore, in all results discussed here, a 200 mT field was applied during the fabrication of the ArtC, as in Fig.2b.

2.3 The effect of material composition and processing conditions on the geometry of ArtC

The aspect ratio is an important geometrical property of the magnetic artificial cilia. Generally, a high aspect ratio is desired, as it helps for the cilia to achieve a bigger deflection during actuation and to generate larger flow speeds or better mixing.[20] The length of the generated cilia depends on two aspects namely the length of the filament at breakup and the amount of filament retraction. The former can be enhanced by introducing strain hardening or extension/shear thickening into the material whereas the latter is affected by the precursor elasticity as well as its surface tension. Because the precursor material is a liquid during the roll-pulling process, the surface tension works against the effort of making high aspect ratio cilia: after the pulled-out filament breaks up, the remaining part collapses under the effect of surface tension. Although the exact pressure field exerted by the surface tension depends on the changing geometry of the cilium and a numerical approach is required to obtain it, a rough estimation can be made based on the Laplace pressure $P = 2\sigma/r$, where σ is the surface tension and r is the radius of curvature. If the surface tension of PDMS (roughly 20 mN/m) is taken for σ, a typical 20 μm diameter filament will experience a Laplace pressure of roughly 4000 Pa. Such a high pressure can dull the tip into a rounded shape while pushing the filament back into the precursor layer, thereby effectively reducing the length of the filament and flattening the surface in a short amount of time. For example if standard PDMS Sylgard 184 (with a viscosity of 3.5 Pa·s) is used, it takes only a fraction of a second for the cilia with the shape of a filament of such size to disappear, as was observed in the experiments. Such a small time window adds complexity to the process, because then the curing of the artificial cilia will have to be done very quickly. Moreover, entangled polymers behave viscoelastically during extension and will cause strain recovery after filament breakup.[26] So the combined effect of surface tension and elastic recovery needs to be countered for the resulting ArtC to maintain a sufficient aspect ratio.

PDMS gum was added to the precursor material to enhance its elongational viscosity, and possibly introduce strain hardening, thereby stabilising the filament against breakup.[27] However, only a marginal effect was observed. To stabilise the generated filaments, silica nanoparticles and PEO-b-PDMS were added to the base PDMS to provide the mixture a yield stress, i.e. under low stress, the material behaves like an elastic solid whereas viscous flow occurs above a certain stress value. In addition, after flow cessation, the material regains its yield stress due to the recovery of the particle network. This rheological property of the mixture helps the formed ArtC to resist collapsing after their formation under the joint effects of fluid elasticity and surface tension, and it makes the process more robust as the curing of the cilia does not need to happen instantaneously. Therefore, it is essential to study the rheology of the material with different compositions, in order to be able to evaluate and improve the fabrication results of ArtC.

In principle, the precursor filament undergoes a combination of shear and extension during the pulling process, with shear probably being more important during the initial stage of the filament generation and close to the substrate. Based on the observations of Khandavalli *et al.*[24] for gravure printing, that the initial shear rate is a more relevant strain rate governing liquid pickup as compared to the initial extension rate, in combination with more extensive possibilities to study time effects, we opted to characterize the precursor materials by means of shear rheology. It should be noted that the shear and extension rates occurring in the process are beyond the measurement range of typical commercial rheometers for shear as well as extension. Nevertheless, characterization of important rheological parameters such as viscosity, yield stress and storage modulus allows to gain qualitative insight in the effects of precursor rheology on the geometry of the generated cilia. Furthermore, fabrication tests were performed with different precursor materials and different processing speeds, while the formation and breakup of the filaments was recorded *in situ* using a high-speed camera.

2.3.1 Shear rheology of different compositions

A stress-controlled shear rheometer (Anton Paar MCR501) with cone-plate 25 mm – 1° was used to characterize the rheological effect of adding silica particles and PEO-b-PDMS copolymer to the precursor mixture. No slip was observed during these tests. In a typical test, first a constant shear rate of 1 s^{-1} was applied for a fixed period of time to remove the shear history of the sample loading, then a small amplitude oscillation was applied, and the evolution of storage and loss modulus over time was recorded. Finally, a step increasing shear stress was applied to the sample to obtain the yield stress (creep tests), with each step lasting for at least 20 minutes. To study the effect of the composition on the precursor rheology, the effect of the silica particle concentration at fixed concentration of PEO-b-PDMS copolymer (11 %vol) and that of the PEO-b-PDMS concentration at a fixed silica concentration (5 %vol) were separately investigated.

The silica particles are known to form a network structure in the PDMS matrix because of their hydrophilic surfaces. This structure brings certain rigidity to the matrix, and can only be broken down when a sufficient amount of stress is applied.[28] As shown in Fig.3a, the yield stress of the mixture increases with increasing concentration of silica particles. The observed power law increase of the yield stress with silica concentration has been reported before, with an exponent of 3.3 ± 0.5,[29] which is smaller than the value of 11.5 observed here. The higher value of the power law exponent could be the result of the presence of the PEO-b-PDMS copolymer (see below). Too many particles may lead to large aggregates,[30] which negatively affect the homogeneity of the precursor mixture and are undesirable in the process of producing micro-structures such as the ArtC. Also from Fig.3a, the viscosity of the precursor increases with more silica particles, and there appears to be a power law relation between the viscosity and the silica volume percentage with an exponent of about 4.3. The viscosity values (Fig.3a) were taken after 5 minutes of shear at a shear rate of 1 s^{-1}.

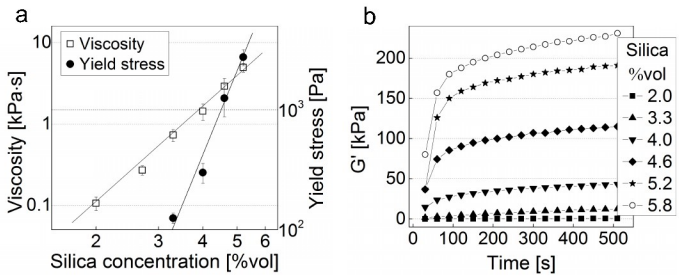

Fig. 3 Results of shear rheological study of precursor materials with different silica concentrations. (a) Shear viscosity at 1/s and yield stress of precursor mixtures with 11.5 %vol PEO-b-PDMS copolymer and varying amount of silica nanoparticles; (b) the change of storage modulus G' over time measured with 1 rad/s angular frequency and 0.05 % amplitude oscillation.

Besides the absolute value of the yield stress, the kinetics of the structure build up is also important in determining the outcome of the fabrication process. After filament breakup, if the structure (hence the yield stress) inside the filament takes too long to build up to a sufficient value to withstand the surface tension, it will not be able to effectively prevent the collapsing of the filament, leading to very small aspect ratios of the ArtC. In order to probe the timescale of the structural buildup inside the precursor mixture using shear rheology measurement, we applied a constant shear rate of $1s^{-1}$ resulting in structure breakdown, followed by small amplitude oscillatory shear (SAOS) and recorded the evolution of the storage modulus G', which reflects structure buildup. Fig.3b shows the G' buildup after the cessation of shear for the precursor material with different silica concentrations. A few observations can be made from the graph. First, it is evident that with the increase of the amount of silica particles, the absolute plateau value of G' increases, which corresponds to the increase of the yield stress. Although the time to reach the plateau value of G' is approximately the same indicating similar buildup kinetics, the slopes of the increase in G' become steeper when more silica particles are added. Hence, the yield stress required to counter the surface tension will be reached faster, which helps to generate cilia with a longer and more slender shape. Second, it can be seen from Fig.3 that the time scale for the yield stress build-

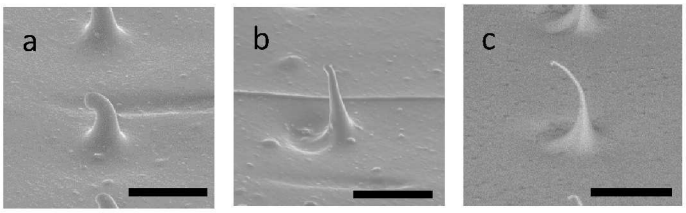

Fig. 4 Geometries of the magnetic artificial cilia with different silica concentrations. As shown from (a-c), the aspect ratio of the artificial cilia increases with increasing loading of silica particles in the precursor mixture, which is 3.3, 4.0 and 4.6 %vol respectively for a, b and c. The PEO-b-PDMS concentration is kept at 11.5 %vol. All scale bars are 200 μm.

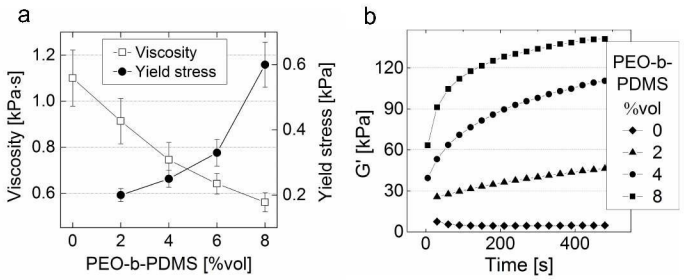

Fig. 5 Results of shear rheological study of different PEO-b-PDMS copolymer concentrations. (a) steady state viscosity at 1/s and yield stress of mixtures with 5 %vol silica and varying amount of copolymer; (b) the change of storage modulus G' over time measured with 1 rad/s angular frequency and 0.05 % amplitude oscillation.

up is typically in the order of tens of seconds, which makes the yield stress unable to counter the elastic effect. As we observed from high speed imaging of the filament pulling process, the elastic snap-back of the filament after breakup happens in a small fraction of a second, which is manifested as a rapid decrease in the length of the filament immediately after breakup. Therefore, the yield stress of the mixture can have little effect on the initial decrease of the filament length caused mainly by the elastic effect, but only works against the surface tension, which is more dominant at a later stage.

Fig.4 shows the typical shapes of the ArtC made with different concentrations of silica particles. With low silica concentrations, the precursor material has a lower yield stress that also builds up slower, so that the filament can not hold its geometry against the surface tension, resulting in a bulged shape (Fig.4a). With more particles added, the final shape became more slender and the total length also became longer (Fig.4b,c), which is beneficial for the magnetic actuation.

In the presence of silica particles, the concentration of PEO-b-PDMS copolymer can also affect the yield stress. The PEO side chains in the PEO-b-PDMS copolymer experience attractive interaction (through hydrogen bonds)[31] with the silica particles, and it is expected that with multiple side chains in a single molecule, bridging between particles is created, thereby effectively reinforcing the structure, leading to a higher yield stress, which is confirmed in Fig.5a. The PDMS backbone of the PEO-b-PDMS makes it miscible with the PDMS base,[32] which could also help to disperse silica particles in the matrix more homogeneously, preventing excessive aggregation, thus being beneficial for creating fine ArtC structures. One the other hand, because the PEO-b-PDMS has a smaller molecular weight (about 3000 g/mol) and hence a lower viscosity than that of the PDMS 184 base, increasing its volume percentage reduces the viscosity of the matrix fluid, which then manifests itself as a drop in the shear viscosity of the mixture. Steady shear viscosity values are shown in Fig.5a.

As increasing the concentration of both the silica nanoparticles and the copolymer can increase the yield stress of the mixture, their opposing effects on viscosity can provide a useful tool to tune the viscosity of the mixture while maintaining the level of yield stress, or vise versa. This is beneficial for the fabrication process as it provides the possibility to fine tune some of the most important rheological parameters. Moreover, as shown in Fig.3a, a relatively small increase in the concentration of silica particles can result in a big jump in both the yield stress and the viscosity, while Fig.5a show a more gradual change of the two parameters when the copolymer concentration is changed. Therefore, the concentration of the silica particles can first be fixed to coarsely set the range of viscosity and yield stress of the mixture, while the copolymer concentration can be changed later on to fine tune the rheological properties. From preliminary experiments, we have found that the silica concentration of 5 %vol provides a suitable range of viscosity and yield stress, and the following fabrication tests were carried out to identify a level of copolymer concentration for 5 %vol of silica that can be used to create ArtC with good geometry. Note that it was not meant to be an exhaustive test to find the optimum composition, but rather to provide an example of the selection process, and the resulting composition found here could potentially be improved even further.

2.3.2 Fabrication tests with different compositions and processing speeds

Apart from the concentration of different components, the speed of fabrication is also an important parameter. It is clear that the rheological response of the precursor material is non-linear and thixotropic, i.e. its viscosity is highly dependent on the value of the applied stress or strain, and on how long these stresses or strains have been applied. Therefore, the substrate speed is also important, as it determines the extension rate of the filaments (see Supplementary Information), hence influences the deformation of the filaments pulled out from the precursor layer and their subsequent break-up, which eventually influence the geometry of the resulting ArtC. In order to obtain a more comprehensive understanding of the effect of the substate speed, *in situ* fabrication tests using different precursor mixtures with various concentrations of PEO-b-PDMS at different speeds were performed.

For the realtime observation and measurement of the filament formation and breakup, a high speed camera (Phantom V9, Vision Research) equipped with a microscope probe lens (Imago Group) was used for image capturing, and the length of the filaments at the point of breakup was measured. In order to obtain clear images, a single row of 200 μm in diameter and 300μm long micropillars was used to provide the filament pullout points, and a mercury lamp equipped with a fibre-optic light guide was used

to provide sufficient illumination in the gap between the roll and the substrate, where the filaments were pulled out.

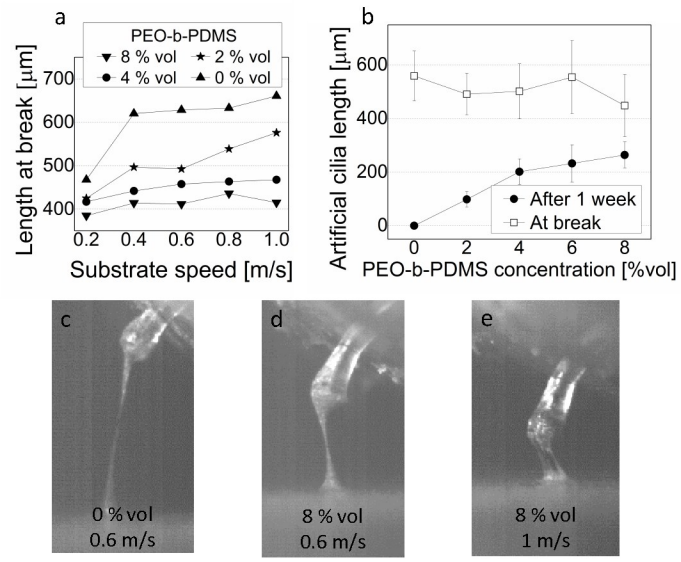

Fig. 6 Results of the fabrication test with precursors of different PEO-b-PDMS concentration at varying processing speeds. (a) Average length of the filaments at the point of break for samples with different amounts of PEO-b-PDMS copolymer. The standard deviation values of the data points are about 20 % (not shown in the graph to avoid excessive overlapping). (b) Comparison of the lengths of the filaments at the time of breakup and after 1 week with the same samples. The substrate speed during the roll pulling process was 0.5 m/s in this case. (c-e) Snapshots of high speed image recordings during the fabrication tests of samples with different amount of PEO-b-PDMS copolymer: (c) no copolymer with a substrate movement speed of 0.6 m/s, (d) 8 %vol copolymer with the same speed, and (e) an example of multiple filaments created from a single contact point at 1 m/s substrate speed with the same sample as (d).

Fig.6a shows the average length at the time of breakup (the breakup length) for precursor materials of varying concentration of PEO-b-PDMS at different processing speeds. It can be seen that the breakup lengths of precursors with lower PEO-b-PDMS copolymer concentrations are larger and increase more significantly when the substrate speed is increased. Note that with low copolymer content, the mixture does not have a high yield stress and can flow more easily. In this case, the mixture can be seen as a viscoelastic fluid and the relation between filament extension limit and the extension rate can be explained by different timescales, e.g. the breakup length increases with the extension rate when the rate of filament extension exceeds the rate of viscoelastic recovery, which was well studied in the past for viscoelastic fluids.[33,34] On the other hand, for precursors with higher PEO-b-PDMS concentrations, the materials become more rigid at rest and higher stresses are needed for flow to occur (higher yield stress). In this case the extension of the filament is more localized in the area with the highest stress, e.g. the area with the smallest cross section, which usually is in the middle part of each filament. This results in a more non-uniform extension, and the filaments will break up earlier, as less material "participates" in the extension. Moreover, elastic behavior emerges at higher speeds for mixtures with higher copolymer loading, a phenomenon also discussed in the literature.[33] Fig.6e shows a typical manifestation of this phenomenon, in which multiple short filaments instead of a single long one were pulled out by one contact point. This type of instability occurs more frequently with the increase of fabrication speed, leading to unstable pulling results and causing a decrease in the average breakup length.

Immediately after the filaments break up, they start to collapse under the combined effect of surface tension and fluid elasticity. Meanwhile, the material starts to build up an inner structure which results in a yield stress that resists the flow and helps the ArtC to maintain a certain length. Therefore, as shown in Fig.6b, although the breakup lengths of the filaments for precursors with less PEO-b-PDMS copolymer were initially longer, the precursors with higher copolymer content were able to retain more of that length and eventually resulted in longer artificial cilia, owing to their higher yield stress and faster structure buildup to counter collapsing. The final lengths were measured after 1 week, to ensure the ArtC had reached their equilibrium length. Note that in these experiments the precursor materials do not contain curing agent, therefore the geometry stabilization was caused solely by their rheological properties. This is important for the robustness of the fabrication process, as the ArtC do not need to be immediately cured to maintain their shapes, instead they can be cured at a later stage of the process.

From the results of the rheological and fabrication studies, it can be concluded that the rheological parameters such as the yield stress, viscosity and elasticity all influence the final geometry of the ArtC from the roll-pulling process. The yield stress in particular plays a dominant role in maintaining the cilia length after filament breakup, and the cilia length can be increased by increasing the amount of silica nanoparticles and PEO-b-PDMS copolymer. In addition, high concentrations of these additives also increase the elasticity of the mixture, which can lead to instabilities during filament pull-out, particularly at high speeds, and reduce the average length of the ArtC. In the above rheological and fabrication study, the effects of the concentration of silica particles and copolymer and the speed of fabrication are investigated, and they have provided better understanding of the process. However, a complete optimisation of the precursor material needs to take more factors into consideration, such as the viscosity of the PDMS base and the amount of curing agent. Moreover, other aspects related to processing could also affect the end result, such as the method of applying the precursor layer onto the substrate, the rest time between the moment the layer is made and the moment the filaments are pulled, the magnetic field intensity during the fabrication process and the curing temperature/time. A complete optimisation of the whole fabrication process is therefore out of the scope of the current study.

Based on the above findings, in the following actuation experiments for the flow generation in a microfluidic chip, a composition of 5 %vol silica particles, 8 %vol PEO-b-PDMS copolymer, 1 %vol silicone gum, 6 %vol iron particles, 73 %vol Sylgard 184 and 7.3 %vol Sylgard 184 curing agent was used for preparing the precursor mixture, and a substrate speed of 0.8 m/s was used during fabrication.

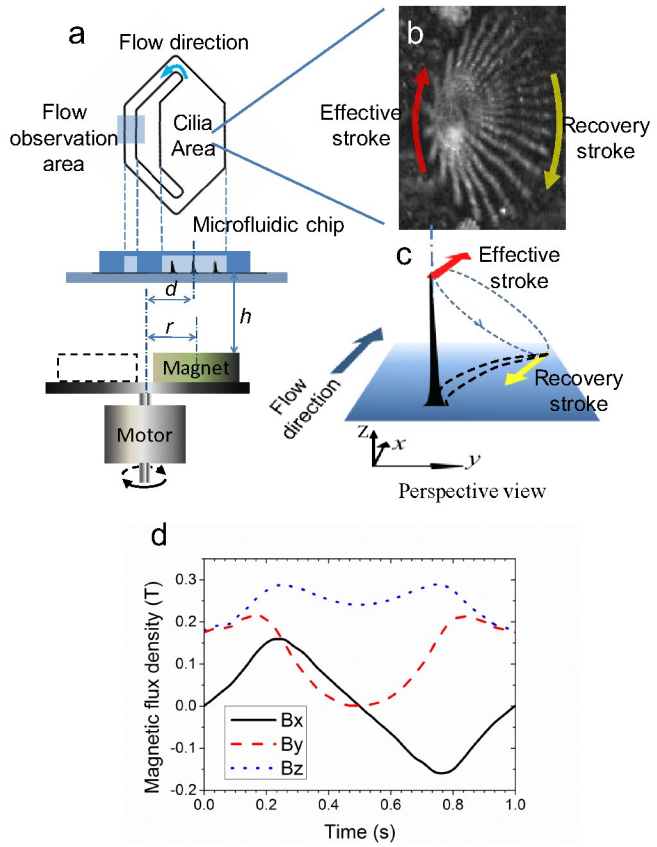

Fig. 7 Actuation scheme of the magnetic artificial cilia. (a) Microfluidic chip with a cilia chamber and a circulation channel for flow observation placed above a rotating magnet with a maximum rotating frequency of 20 Hz; the rotation axis of the magnet is offset by a distance d with respect to the centre of the cilia chamber, and the magnet is placed at a distance r from the rotation axis; The total area of the cilia chamber is 8 mm^2, and the width of the recirculation channel is 500 μm; (b) top view image of the motion of one rotating artificial cilium showing the tilted cone rotation, composed of 25 frames in one actuation cycle at 1Hz; (c) schematic drawing of cilia rotation in perspective view; (b) and (c) have arrows indicating the effective stroke, when cilia are moving in a more upright position, the recovery stroke, when they are closer to the substrate, and the resulting overall flow direction; (d) simulation result of the three components of the periodically changing magnetic flux density experienced by artificial cilia during one actuation cycle, with d = 6 mm, r = 6 mm and h = 2 mm, actuated using a 10 mm high, 20 mm diameter cylindrical magnet with a remnant flux density of 1.3 T. Illustrations are not to scale.

3 Actuation and flow generation

As shown in Fig.7a, a recirculation microfluidic chip made of PDMS was used to characterize the flow generation capacity of the artificial cilia, similar as described in our earlier work.[23] The chip contains a cilia chamber, in which the ArtC are integrated in various configurations, and a recirculation channel in which the generated flow can be observed. A rotating magnet was placed underneath the cilia with its rotation axis at an offset (Fig.7a) with respect to the centre of the cilia chamber. This way, a time-dependent magnetic field was generated (Fig.7d) that actuates the cilia to perform a tilted conical motion, which is similar to the motion of some natural cilia and that in several previous studies on artificial cilia.[22,23,35] In this motion, the paths of the cilia are not time-reversible because of their asymmetry with respect to the normal of the surface. Such a so called non-reciprocal motion is able to generate a net fluid flow in low Reynolds number environments.[36] In a typical experiment, the length of the cilia is around 250 μm, and the inner height of the chip is 420 μm. The complete ArtC fabrication process, as well as the fluid actuation experiment, are illustrated in an animation in the online Video Abstract.

The effect of ArtC configuration and fluid viscosity on the flow generation was studied, as shown in Fig.8. The flow speeds were characterized for two fluids with different viscosities, namely deionized water (1 mPa·s at room temperature) and a 60 wt% glycerol solution (10 mPa·s at room temperature). The flow was visualized by seeding the fluids with 3 μm polystyrene particles and the speeds were measured in the recirculation channel indicated in Fig.7a. A high speed camera connected to a stereo microscope was used to record the seeding particle movement and the fluid flow speed was obtained by calculating the average speed of the particles in the geometrical centre of the channel over 120 seconds. The number of cilia was varied by changing the number of rows and columns from 3 to 5 resulting in 9,14 or 25 cilia in the cilia chamber.

Several observations can be made from the results of the measured fluid flow velocities in these settings. First, the flow speeds generated in glycerol solution were lower than that in water, because the ArtC experienced higher viscous drag in glycerol solution and hence followed a smaller cone, which caused the decrease in the generated flow speed. As shown in previous studies, the flow speed generated by the tilted conical motion of ArtC is proportional to $f\alpha sin\Theta sin^2\Psi$, with f being the actuation frequency, α being the aspect ratio of the cone, Θ the tilt angle of the cone and Ψ the cone opening angle.[23,37] With a larger viscous torque applied to the moving cilia by either a faster movement or a higher viscosity of the medium, the opening angle of the cone Ψ becomes smaller and thus the flow speed decreases.[23] Second, a larger number of cilia generate higher flow rates at the same actuation frequency, which can be naturally explained by the fact that there are more cilia to drive the flow. However, the results also show that the flow increased less from the 4×4 setting to the 5×5 setting than for an increase from 3×3 to 4×4. This means that with increasing cilia number the gain of the flow speed is diminishing, and the relationship between the number of cilia and the induced flow rate is non-linear. This may result from hydrodynamic interactions between the cilia, which may suppress the effectiveness of flow generation of each beating cilia. Or it could result from the geometry of the device, which is tapered at the entrance of the recirculation channel. This geometry could make the cilia closer to the sides less effective than the ones in the middle in sending the flow into the recirculation channel. Hence, a change in the layout of the cilia may further enhance the flow speeds. Such an optimisation is however beyond the scope of the present work. Finally, the flow generated with water has a larger than linear increase with respect to the actuation frequency, which is different from the glycerol solution, for which the relationship is a little less than linear. The latter is consistent with the flow speeds

generated by the artificial cilia in a previous study.[23] One possible explanation for a greater-than-linear increase of flow speed with respect to the actuation frequency could be the presence of inertial effects. If we compute the local Reynolds number $Re = \rho v L/\eta$ using the density of water for ρ, dynamic viscosity of water for η (1 mPa·s), the length of cilia for L (250 μm) and the moving speed of the cilia tips at 20 Hz for v (around 0.02 m/s, as observed from high speed imaging), the result for Re is around 6, which is in the range where inertial effects can indeed influence the flow generated by the cilia, as reported in another study.[38] We expect that the flow speed will start to decrease if the rotation frequency becomes larger than a certain threshold value, like in the case shown in our previous work.[23] The reason for this decrease is that the cilia experience an increasing hydrodynamic drag as the rotation frequency becomes larger, which causes the motion of the cilia to diminish, and the flow generated by the ArtC will peak at a threshold frequency.[22,23] However in this study, a different magnetic actuation setup from our previous work[23] is used and the highest frequency reachable of the current actuation setup is 20 Hz, and the threshold frequency was not reached, which means that still higher flow rates are possible by using an improved magnetic actuation setup.

It is worthwhile to compare the performance in flow generation of the ArtC developed in this study with other microfluidic pumping methods. One important criterion is the maximum flow rate Q_{max}, which can be roughly estimated based on the flow speed observed in the recirculation channel.[23] For the 5×5 ArtC configuration in water, a Q_{max} of about 0.7 μL/min was obtained in the recirculation channel. This is comparable to the flow rate generated by electrohydrodynamic and electroosmotic pumping methods.[39] As mentioned, it can be improved by optimising materials and geometrical design, and by using an improved magnetic actuation setup. Another characteristic measure is the self-pumping frequency f_{sp}, which is Q_{max} divided by the total size of the pump S_p.[39] If we take the size of the cilia chamber as S_p, which is about 8×10^{-3} cm^3, then an f_{sp} of about 0.2 min^{-1} is obtained, which is also comparable to other methods, especially for pumps that are only able to generate a small pressure difference, such as the artificial cilia.[39] See the Supplementary Information for more details about the comparison.

4 Conclusion

In this paper, a novel magnetic field assisted roll-pulling process for magnetic ArtC fabrication is presented. Slender cone-shaped ArtC were produced, with their spatial arrangement pre-defined by the micropillars on the roll surface. The size of the cilia array, which is mostly restricted by the length of the roll, can potentially be scaled up to facilitate large area production, as has been demonstrated in Fig.1d and ESI. The fabrication speed can go up to 1 m/s in our experiments, which is restricted by the speed limit of the substrate. Such a high speed combined with the large production area provides the opportunity to scale up the fabrication of artificial cilia towards the realization of industrial applications.

In order to understand the effect of material composition and processing parameters on the geometry of ArtC, the shear rheology of a variety of precursor compositions was investigated.

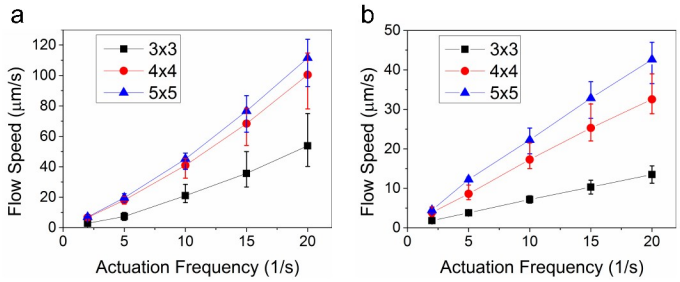

Fig. 8 Flow speeds observed in the recirculation channel versus the actuation frequency in (a) water and (b) 60 wt% glycerol solution. Movies of the actuation as well as the flow generated in the recirculation channel, are presented in the ESI. It can be seen from the movies that at lower frequencies, the flow in the channel shows pulsatile behavior but on average forms a net flow, and at higher frequencies the pulsatile nature becomes insignificant and a continuous flow is observed.

Shear viscosity, yield stress and storage modulus buildup after cessation of shear were measured and the underlying mechanisms for the observed differences were discussed. It was found that higher PEO-b-PDMS content resulted in a lower steady shear viscosity while having higher silica content increased the viscosity. Meanwhile, increasing either PEO-b-PDMS or silica content resulted in higher storage modulus and higher yield stress. Moreover, *in situ* fabrication tests were carried out and the correlation between fabrication results and the rheology test results was assessed. It was found that artificial cilia made with compositions that have higher PEO-b-PDMS content retain more of their lengths after breakup of the pulled-out filaments, although their initial filaments breakup lengths were smaller, which resulted in higher aspect ratio ArtC.

The ArtC fabricated in this process are capable of generating fluid pumping in a closed loop microfluidic channel with external magnetic actuation. Using a rotating magnet, a maximum flow speed of about 120 μm/s was achieved in the centre of the recirculation channel with a cross section of 500 μm wide and 420 μm high when the ArtC were actuated in water at the frequency of 20 Hz. The flow rate and self-pumping frequency of ArtC are comparable to those obtained by other microfluidic pumping methods in the literature. The advantages of artificial cilia pumping are that it is a fully integrated solution, it allows for local flow control, and the effect is obtained by an external magnetic field without the need for any physical connection to the microfluidic chips (e.g. pneumatic or electrical).

It is worth mentioning that apart from a 3D rotational motion, the ArtC can also be actuated into a 2D planar motion, where the effective and recovery strokes have different paths, resulting in an asymmetric motion which can generate a net flow.[10] In fact, a combination of the two types of asymmetry would potentially be more effective for flow generation, meaning that the ArtC remains straight during the effective stroke but curls back during the recovery stroke in the rotational motion shown in this paper.

The effectiveness of the ArtC and the scalable and cost-effective production process make this work a promising technological platform for application development. Besides pumping, the ability of ArtC to manipulate fluids could also be used in other appli-

cations, for example in mixing of different fluids in a low Reynolds number environment, or in anti-fouling for submerged sensors by actively repelling contaminants from their surfaces. It is also interesting to study the performance of ArtC in non-Newtonian fluids, which could be important for applications that involve biological fluids. One distinction of using ArtC against other pumping methods is that they can create local flow fields without physical connection to the device, such as fluid inlet/outlets and electrodes, which could provide potential benefit for creating flow in closed systems. With regard to the process itself, the geometry of ArtC may be further optimised by formulating alternative precursor materials and by carrying out more extensive rheological studies, preferably using extensional rheometers that can reach a high rate of deformation.

Ackowledgement

This research forms part of the research programme of the Dutch Polymer Institute DPI, project #689. We would like to thank I. Meijer for her contribution to the rheology part of this work, and Equipment and Prototype Center at TU Eindhoven for the construction of the roll-pulling setup.

References

1 L. T. Haimo and J. L. Rosenbaum, *The Journal of cell biology*, 1981, **91**, 125–130.

2 E. Arzt, S. Gorb and R. Spolenak, *Proceedings of the National Academy of Sciences of the United States of America*, 2003, **100**, 10603–6.

3 X. Gao and L. Jiang, *Nature*, 2004, **432**, 36–36.

4 J. M. den Toonder and P. R. Onck, *Trends in Biotechnology*, 2013, **31**, 85–91.

5 B. A. Evans, A. R. Shields, R. L. Carroll, S. Washburn, M. R. Falvo and R. Superfine, *Nano letters*, 2007, **7**, 1428–34.

6 M. Vilfan, A. Potocnik, B. Kavcic, N. Osterman, I. Poberaj, A. Vilfan and D. Babic, *Proceedings of the National Academy of Sciences of the United States of America*, 2010, **107**, 1844–1847.

7 A. Babataheri, M. Roper, M. Fermigier and O. Du Roure, *Journal of Fluid Mechanics*, 2011, **678**, 5–13.

8 J. den Toonder, F. Bos, D. Broer, L. Filippini, M. Gillies, J. de Goede, T. Mol, M. Reijme, W. Talen, H. Wilderbeek, V. Khatavkar and P. Anderson, *Lab on a chip*, 2008, **8**, 533–41.

9 J. Belardi, N. Schorr, O. Prucker and J. Rühe, *Advanced Functional Materials*, 2011, **21**, 3314–3320.

10 J. Hussong, N. Schorr, J. Belardi, O. Prucker, J. Rühe and J. Westerweel, *Lab on a chip*, 2011, **11**, 2017–2022.

11 R. Dreyfus, J. Baudry, M. L. Roper, M. Fermigier, H. A. Stone and J. Bibette, *Nature*, 2005, **437**, 862–865.

12 C. L. van Oosten, C. W. M. Bastiaansen and D. J. Broer, *Nature materials*, 2009, **8**, 677–682.

13 L. D. Zarzar, P. Kim and J. Aizenberg, *Advanced materials*, 2011, **23**, 1442–6.

14 M. Yang, N. Sniadecki and C. Chen, *Advanced Materials*, 2007, **19**, 3119–3123.

15 H. Bellanger, T. Darmanin, E. Taffin de Givenchy and F. Guittard, *Chemical Reviews*, 2014, **114**, 2694–2716.

16 N. J. Sniadecki, A. Anguelouch, M. T. Yang, C. M. Lamb, Z. Liu, S. B. Kirschner, Y. Liu, D. H. Reich and C. S. Chen, *Proceedings of the National Academy of Sciences*, 2007, **104**, 14553–14558.

17 S. Große and W. Schröder, *Measurement Science and Technology*, 2008, **19**, 015403.

18 P. J. Glazer, J. Leuven, H. An, S. G. Lemay and E. Mendes, *Advanced Functional Materials*, 2013, **23**, 3016–3016.

19 K. Liu and L. Jiang, *Annual Review of Materials Research*, 2012, **42**, 231–263.

20 F. Fahrni, M. W. J. Prins and L. J. van IJzendoorn, *Journal of Magnetism and Magnetic Materials*, 2009, **321**, 1843–1850.

21 S. N. Khaderi, C. B. Craus, J. Hussong, N. Schorr, J. Belardi, J. Westerweel, O. Prucker, J. Rühe, J. M. J. den Toonder and P. R. Onck, *Lab on a chip*, 2011, **11**, 2002–10.

22 Y. Wang, Y. Gao, H. Wyss, P. Anderson and J. den Toonder, *Lab on a chip*, 2013, **13**, 3360–6.

23 Y. Wang, Y. Gao, H. M. Wyss, P. D. Anderson and J. M. J. den Toonder, *Microfluidics and Nanofluidics*, 2014, **18**, 167–174.

24 S. Khandavalli, J. Alex Lee, M. Pasquali and J. P. Rothstein, *Journal of Non-Newtonian Fluid Mechanics*, 2015, **221**, 55–65.

25 J. Vermant, G. Cioccolo, K. Golapan Nair and P. Moldenaers, *Rheologica Acta*, 2004, **43**, 529–538.

26 V. C. Barroso, R. J. Andrade and J. M. Maia, *Journal of Rheology*, 2010, **54**, 605.

27 D. F. James, *Annual Review of Fluid Mechanics*, 2009, **41**, 129–142.

28 L. E. Kosinski and J. M. Caruthers, *Journal of Non-Newtonian Fluid Mechanics*, 1985, **17**, 69–89.

29 J.-M. Piau, M. Dorget, J.-F. Palierne and A. Pouchelon, *Journal of Rheology*, 1999, **43**, 305–314.

30 M. I. Aranguren, *Journal of Rheology*, 1992, **36**, 1165.

31 Q. Zhang and L. a. Archer, *Langmuir*, 2002, **18**, 10435–10442.

32 R. M. Hill, *Silicone Surfactants*, Taylor & Francis, 1999.

33 A. Y. Malkin and C. J. S. Petrie, *Journal of Rheology*, 1997, **41**, 1–25.

34 M. Yao, S. H. Spiegelberg and G. H. McKinley, *Journal of Non-Newtonian Fluid Mechanics*, 2000, **89**, 1–43.

35 A. R. Shields, B. L. Fiser, B. A. Evans, M. R. Falvo, S. Washburn and R. Superfine, *Proceedings of the National Academy of Sciences*, 2010, **107**, 15670–15675.

36 D. J. Smith, J. R. Blake and E. A. Gaffney, *Journal of the Royal Society, Interface / the Royal Society*, 2008, **5**, 567–73.

37 M. T. Downton and H. Stark, *EPL (Europhysics Letters)*, 2009, **85**, 44002.

38 M. Baltussen, P. Anderson, F. Bos and J. den Toonder, *Lab on a chip*, 2009, **9**, 2326–31.

39 D. J. Laser and J. G. Santiago, *Journal of Micromechanics and Microengineering*, 2004, **14**, R35–R64.